However, such processes should produce a hydrogen cloud with a radius larger than 2.5 R_S and therefore could not account for the observed B ring emission.

Saturn emission. The ultraviolet photometer scanned across Saturn's disk during the period from 1000 to 1400 on day 244, when the spacecraft was about 7.2 to 3.5 R_S from Saturn. During this period, the equatorial region of Saturn's disk was in the field of view at a clock angle of ~ 170°, and the whole disk subtended an angle that varied from 30° to 60° (Fig. 7). The observations show Saturn emissions with a strong latitudinal variation superimposed on a slowly varying background (Fig. 8). The emissions around Saturn's polar regions appear stronger than the emission from the equatorial region. This variation could result from limb brightening of Saturn's disk or auroral emission due to particle precipitation in Saturn's atmosphere.

Possible emissions due to helium and perhaps atomic ions have also been detected. However, due to high background noise in our short-wavelength channel, these emissions cannot be positively identified without further data analysis. In addition, photochemical and radiative transfer calculations for Saturn's atmosphere are required to properly interpret the long- and short-wavelength observations.

D. L. JUDGE
F.-M. WU
Department of Physics, University of Southern California, Los Angeles 90007
R. W. CARLSON
Jet Propulsion Laboratory, Pasadena, California 91103

References and Notes

1. D. L. Judge and R. W. Carlson, *Science* **183**, 317 (1974).
2. R. W. Carlson and D. L. Judge, *J. Geophys. Res.* **79**, 3623 (1974).
3. H. Weiser, R. C. Vitz, H. W. Moos, *Science* **197**, 755 (1977).
4. E. S. Barker, personal communication.
5. L. A. Frank, personal communication.
6. L. C. Lee, in preparation.
7. W.-H. Ip, *Astron. Astrophys.* **70**, 435 (1978).
8. R. W. Carlson, *Bull. Am. Astron. Soc.* **11**, 557 (1979).
9. N. C. Wickramasinghe, *Intersteller Grains* (Chapman & Hall, London, 1967).
10. ——— and D. A. Williams, *Observatory* **88**, 72 (1968).
11. F.-M. Wu, D. L. Judge, R. W. Carlson, *Astrophys. J.* **225**, 325 (1978).
12. A. F. Cheng and L. J. Lanzerotti, *J. Geophys. Res.* **83**, 2597 (1978).
13. We gratefully acknowledge the support that we received throughout this mission from the Pioneer Program Office at NASA headquarters and the Project Office at the NASA/Ames Research Center under the most able direction of C. Hall. We also thank TRW for providing such a reliable spacecraft and Analog Technology Corporation for providing an ultraviolet photometer with the longevity required for a mission to Saturn. Supported by NASA contract NAS 2-6558 with the NASA/Ames Research Center.

3 December 1979

Imaging Photopolarimeter on Pioneer Saturn

Abstract. *An imaging photopolarimeter aboard Pioneer 11, including a 2.5-centimeter telescope, was used for 2 weeks continuously in August and September 1979 for imaging, photometry, and polarimetry observations of Saturn, its rings, and Titan. A new ring of optical depth* $< 2 \times 10^{-3}$ *was discovered at 2.33 Saturn radii and is provisionally named the F ring; it is separated from the A ring by the provisionally named Pioneer division. A division between the B and C rings, a gap near the center of the Cassini division, and detail in the A, B, and C rings have been seen; the nomenclature of divisions and gaps is redefined. The width of the Encke gap is 876 ± 35 kilometers. The intensity profile and colors are given for the light transmitted by the rings. A mean particle size* $\lesssim$ *15 meters is indicated; this estimate is model-dependent. The D ring was not seen in any viewing geometry and its existence is doubtful. A satellite, 1979 S 1, was found at 2.53 ± 0.01 Saturn radii; the same object was observed ~ 16 hours later by other experiments on Pioneer 11. The equatorial radius of Saturn is 60,000 ± 500 kilometers, and the ratio of the polar to the equatorial radius is 0.912 ± 0.006. A sample of polarimetric data is compared with models of the vertical structure of Saturn's atmosphere. The variation of the polarization from the center of the disk to the limb in blue light at 88° phase indicates that the density of cloud particles decreases as a function of altitude with a scale height about one-fourth that of the gas. The pressure level at which an optical depth of 1 is reached in the clouds depends on the single-scattering polarizing properties of the clouds; a value similar to that found for the Jovian clouds yields an optical depth of 1 at about 750 millibars.*

The imaging photopolarimeter (IPP) is a pointable telescope with an aperture of 2.5 cm that utilizes the spin motion of the spacecraft to scan across an object. It may be stepped in a direction perpendicular to that of the spacecraft's spin, thus forming a two-dimensional map. There are two wavelength passbands, 390 to 500 nm and 595 to 720 nm. The specifications of the instrument were published for Pioneer 10 (*1*) and they are essentially the same for Pioneer 11 (*2*). A detailed description of the polarimeter has been published (*3*); the results for Jupiter and interplanetary particles have been overviewed and are referenced in (*4*). Our Saturn flyby operations have been described (*5*). Geometric characteristics of our spin-scan imaging data will be discussed in detail elsewhere (*6*).

After 6½ years in space, including the active operations during the flyby of Jupiter, the instrument performed remarkably well during the encounter with Saturn. Irregularities in the stepping of the telescope (*2*) occurred, but nearly all the images can be restored. The aperture wheel, which is the other moving component in this instrument, has functioned almost perfectly. No appreciable degradation has been seen during the Saturn encounter in Channeltron detector sensitivity or in optical transmission; we have not noticed any effects of Saturn's particle radiation.

Our inventory of data is shown in Table 1. The total number of Saturn images (0.03° aperture) is 440, and 40 of these have a resolution better than the best resolution of ground-based observations (taken as 1200 km); in terms of pixel width, the highest resolution we attained on Saturn was 90 km. For Titan there are five images with a resolution of ~ 180 km.

The Pioneer image converter system (PICS), designed and built at the University of Arizona, was located at Ames Research Center; it allowed the observing team to monitor the imaging data as well as the instrument's operation for subsequent modification of commands to the IPP. The PICS converted the imaging data to color television signals for nationwide programs of the Public Broadcasting System.

Figure 1 shows a full view of the Saturn system. The rings are seen in scattered light; this is different from the view from Earth, where the rings are usually seen in reflected light. During the flyby the sun illuminated the south side of the rings at a small angle (~ 3°) from the ring plane. Pioneer 11 approached from the north on its long transfer trajectory from Jupiter, which had carried it 1.1 AU out of the ecliptic plane, and the planet was observed from the north except between the times of the ring plane crossings (± 2 hours from the time of closest approach on 1 September 1979). When seen in scattered light, a ring or a division may be dark because of either large or small optical depth (τ). A bright ring in scattered light implies an intermediate optical depth. At the present geometry, maximum brightness occurs at $\tau = 0.06$.

The rings are seen in greater detail in Fig. 2. Table 2 is a summary of the rings and divisions, together with our measurements of their distances from the center in terms of Saturn radii (R_S). Our absolute radius scale for Fig. 2 is based on a fundamental measurement of the outer C ring radius in another image [31 August 1979, 0916 UT, Earth received time (ERT)] that contains both Saturn and the C ring. The numbers in Table 2 are good to $\pm$ 0.011 R_S (we use standard deviations in this report); the cumulative uncertainties are $\pm$ 500 km in R_S, $\pm$ 300 km in the C ring fit, and $\pm$ 300 km in the fits in Fig. 2.

A special observation of the Encke gap was made with the 0.5° aperture between 1614 and 1631 ERT on 1 September, when the spacecraft was underneath the ring plane. The IPP was then observing the light of Saturn transmitted through the rings; the rings themselves were illuminated by the sun, but their brightness was much less than that of Saturn. The width of the Encke gap was found to be 876 $\pm$ 35 km. See (*7*) for a comparison with Earth-based results.

A plot of brightness of the rings is given as a function of distance from Saturn in Fig. 3. Mimas—with Tethys, since their orbits are coupled—seems to dominate the major ring features with commensurabilities lying just inside regions of lower optical depth.

Next we describe the ring system as we have learned to see it in various frames and geometries, including images showing the light of Saturn transmitted through the rings, as seen in Fig. 4.

The controversial D ring cannot be seen in any of our scans, neither in transmitted light nor in the shadow of the rings on the planet as in Fig. 4. We conclude that the D ring did not exist at the time of the flyby, because we did not see it under viewing conditions that are more revealing than those of the discovery claim. The D ring was suggested by Guérin (*8*) because he saw a darker region, sometimes called the Guérin division, at the inside of the C ring on high-resolution photographs taken at the Pic-du-Midi Observatory. Were it not for this darker region, the D ring might have been interpreted as scattered light from the planet; an Earth-based estimate (*9*) of optical depth was 0.3 $\pm$ 0.1. We conclude that the optical depth is < 0.002. The Guérin division may have appeared as a result of adjacency effects (*10*) in the photographic emulsion used by Guérin.

About one-fourth of the way out from the inner boundary of ring C a dark lane

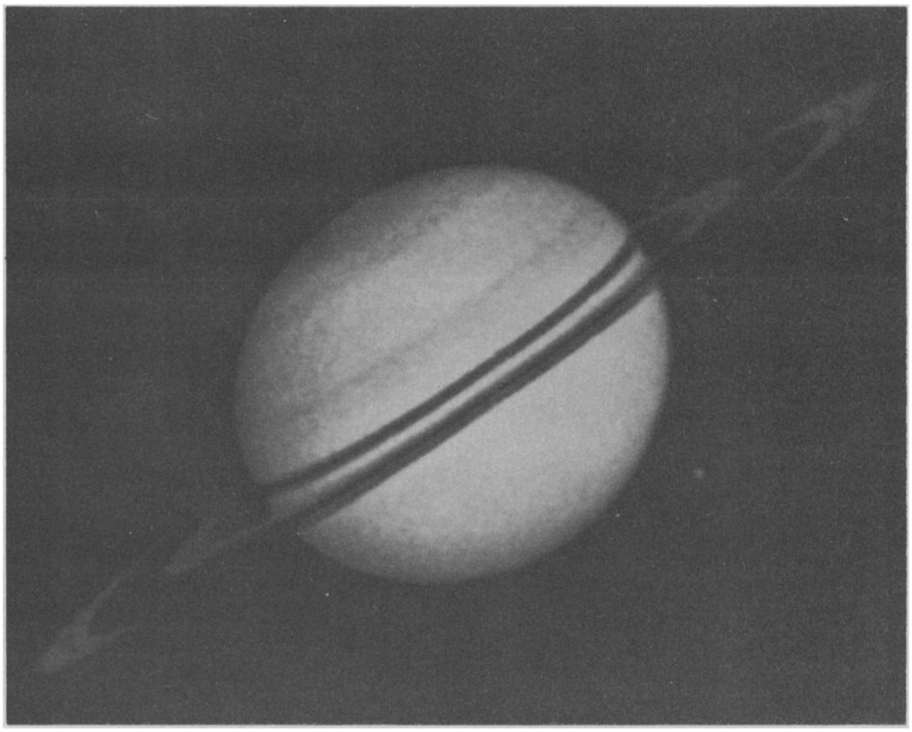

Fig. 1. Image of the Saturn system taken in the red channel on 30 August 1979 at 0533 ERT; range, 2,579,000 km; subspacecraft latitude, + 5.3°; phase angle, 15.6°. The part of the image at the lower left on the A ring was taken, by computer duplication, from the appropriate data at the upper right. The satellite is Rhea. In this image and those in Figs. 2 and 4, north is up and the rotation is from left to right.

Table 1. Observing schedule of the imaging photopolarimeter. The time is given in days (d) or hours (h) before (−) or after (+) Pioneer 11's closest approach to Saturn on 1 September 1979, at 1800 ERT, UT. The range is given in Saturn equatorial radii (R_S = 60,000 km) from the target's center. The phase is the sun-target-spacecraft angle. Mode refers to polarimetry (P) with 0.5° by 0.5° resolution, or imaging (I) with 0.03° by 0.03° resolution.

Time	Target	Range (R_S)	Phase (deg)	Mode
-22^d to -7^d	Saturn plus rings	301 to 113	20 to 19	P,I
-22^d to -7^d	Satellites	301 to 113	20 to 19	P
-7^d to -1^d	Saturn plus rings	112 to 20	19 to 8	P,I
-7^d to -1^d	Satellites	112 to 20	19 to 8	P
-24^h to -15^h	Saturn plus rings	20 to 14	10 to 15	P,I
-14^h	Dione	10	29	P
-13^h to -5^h	Saturn plus rings	13 to 6	9 to 20	P,I
-5^h to -2.5^h	Saturn plus rings	5.6 to 3.4	28	P,I
-2.5^h to -2^h	Saturn plus rings	3.1	51	P
-1.7^h to -1.3^h	Saturn plus rings	2.6	70	P
-1.3^h to -0.7^h	Saturn plus rings	2.2	90	P
-0.7^h to -0.4^h	Saturn plus rings	1.8	90 to 151	P
-0.4^h to 0^h	Saturn plus rings	1.4	151	P
$+1.8^h$ to $+2.4^h$	Saturn plus rings	3.1	151	I
$+2.4^h$ to $+2.8^h$	Saturn plus rings	3.5	130 to 150	P
$+3^h$ to $+4^h$	Saturn plus rings	4.3	130	P
$+4^h$ to $+5^h$	Saturn plus rings	5.1	120	I
$+5^h$ to $+7^h$	Saturn plus rings	6.4	114	P
$+8^h$ to $+12^h$	Saturn plus rings	8 to 12	90 to 115	P,I
$+12.5^h$	Rhea	7	52	P
$+13^h$ to $+17^h$	Saturn plus rings	14	90 to 105	P,I
$+17.5^h$	Titan	9	28	I
$+19^h$	Dione	15	71	P
$+19^h$ to $+23^h$	Saturn plus rings	17 to 21	93 to 91	P,I
$+24^h$ to $+26^h$	Titan	6	23 to 32	I
$+27^h$	Saturn plus rings	23	90	P
$+28^h$	Titan	6	42	P
$+30^h$	Saturn plus rings	25	90	P
$+31^h$	Titan	7	55	P
$+32^h$	Saturn plus rings	26	89	P
$+32^h$ to 4^d	Saturn plus rings	26 to 67	88 to 83	P,I
$+32^h$ to 4^d	Satellites	26 to 67	88 to 83	P
$+20^d$	Saturn plus rings	267	80	P

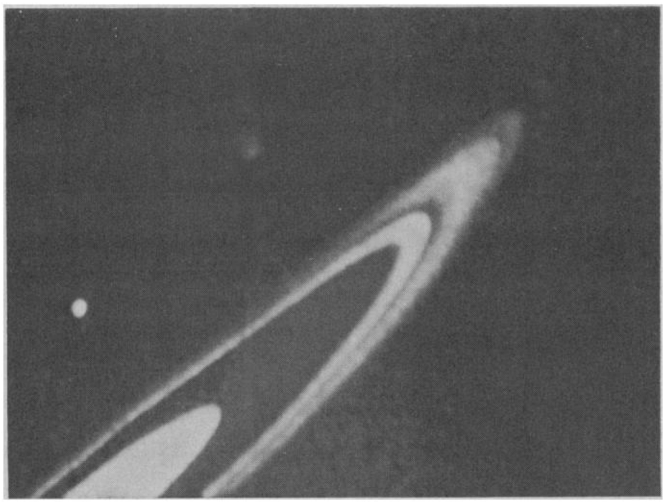

Fig. 2. This is the discovery picture of the F ring and of satellite 1979 S 1. Red channel; 1 September 1979; 0025 ERT; range, 943,000 km; latitude, + 4.6°; phase, 8.6°.

followed by a bright one are seen, and two-thirds out in ring C there is another dark lane and then a bright lane. Other minor features may also be seen. Although there seems to be some longitudinal structure, we cannot rule out the possibility that this is due to noise since the counts are low. A division between the B and C rings is clearly seen when planetary light is transmitted through the rings, as in Fig. 4. This division was probably discovered by Dawes (*11*), but it was not a clear discovery that was generally accepted. The French astronomer Dollfus, and also Lyot before him, had recorded its existence, and the name French division or Dollfus division might therefore be appropriate.

The B ring appears to be dark in our images, but an appreciable amount of light is actually observed in various places; this will be analyzed below.

The Cassini division is bright because it apparently contains enough material to diffusely scatter sunlight efficiently. Structure within it is evident. A narrow gap, showing less scattered light, is located near the center.

The A ring has considerable structure. There seems to be relatively high optical depth just outside the Cassini division, possibly because of the accumulation of particles just outside this apparent dynamical barrier. Next outward there are minor features, followed by the Encke gap.

We propose to use the name division for the wide separations of major rings that have very different optical thicknesses. The prototype is the Cassini division. We propose then that a narrow gap be no longer denoted as a division and that we speak of the Encke gap, rather than the Encke division.

The F ring was discovered by the IPP as a narrow feature (< 800 km wide in our observations) at 2.33 R_S. The optical depth is $\lesssim 2 \times 10^{-3}$; but we see indications of clumpiness in the F ring, in which case the optical depth is that of the clumps. We propose to name the division between the F and A rings the Pioneer division in honor of NASA's Pioneer Project, which made the discovery possible.

The E ring is too faint to be detected by IPP observations; the numbers in Table 1 are from other sources (*12*). Separating the E and F rings seems appropriate because the optical thickness of the E ring is at least 100 times less than that of the F ring, while there is at least one "division" outside the F ring, as seen in the fluxes of energetic particles (*13*).

The sunlight transmitted through the rings is less red than that reflected by the planet. Ratios of counts in the red and blue channels, with uncertainties of ± 0.1, were as follows: Saturn, 2.7; A ring, 2.4; Cassini division, 2.5; and C ring, 2.1. The phase function of the ring particles does not appear significantly different in the blue and red channels of the IPP. In both colors it seems consistent with scattering by spheres that have perfectly diffusing surfaces (Lambert spheres). These two facts seem to indicate that the scatterers are larger than the wavelengths of observation.

The brightness of the B ring is still too great to be consistent with models of the ring based on the brightness observed from Earth on the sunlit side. Earth-based results (*14*) require that the optical depth of the B ring be at least 1.0; this, however, gives only about one-tenth the brightness that we observe from the opposite side. We considered the possibility of illumination of the dark side by "Saturn-shine," but found that this effect would not give rise to a single count at the gain we used. In addition, the observed brightness is patchy, showing radial and possibly longitudinal structure. The variation of brightness is too great to be explained either by stray light or by counting statistics. We conclude that it arises from inhomogeneities in the ring. The light we see leaks through the thick ring at its thinner spots.

We can quantify this with a simple model of the B ring wherein the optical depth has a bimodal distribution. The

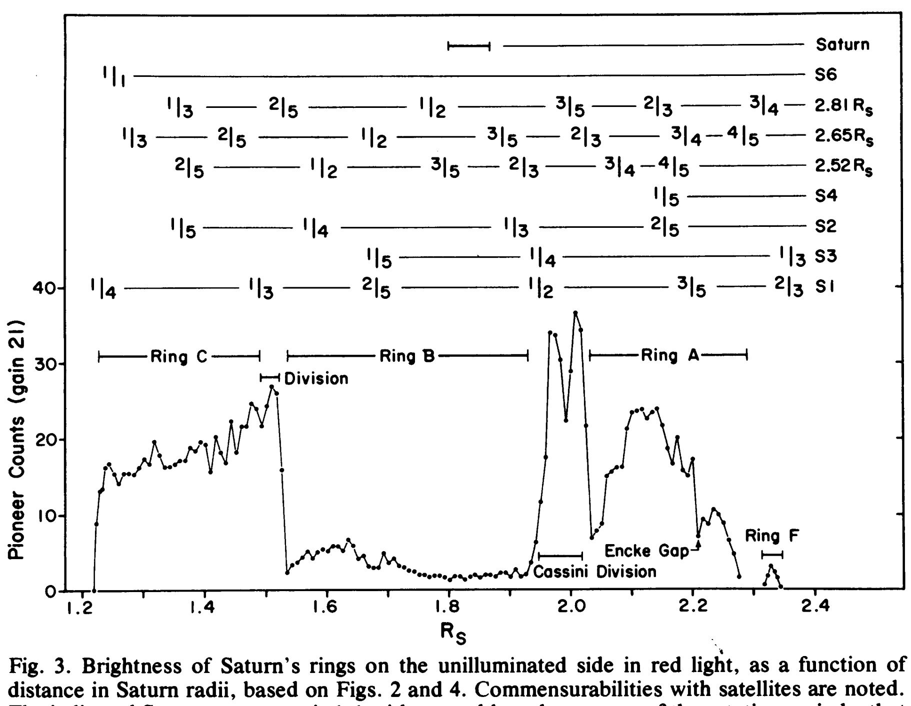

Fig. 3. Brightness of Saturn's rings on the unilluminated side in red light, as a function of distance in Saturn radii, based on Figs. 2 and 4. Commensurabilities with satellites are noted. The indicated Saturn resonance is 1:1 with ground-based measures of the rotation periods; that of Titan is 1:1 with its apsidal motion. Abbreviations: *S1*, Mimas; *S2*, Enceladus; *S3*, Tethys; *S4*, Dione; and *S6*, Titan.

thin component gives rise to almost all the light seen by the IPP, and the thicker component provides the brightness observed from the sunlit side. Because the brightness depends on the optical depth in a different way for each of the various types of observations from Pioneer (ring shadow on the ball, Saturn seen through the rings, dark-side ring brightness), the IPP and Earth-based measurements constrain the parameters of the model. This analysis shows that in at least 5 percent of the surface area of the B ring the optical depth is less than 0.25. (At present we cannot determine whether these areas are totally randomly distributed, or organized into gaps too narrow for our instrument to resolve.) In the rest of the ring the optical depth must exceed 1.5 to match the Earth-based observations.

An upper limit on the particle size can be obtained in conjunction with the Pioneer estimate of an upper limit to mass (*15*). The optical depth of the ring is $\tau = n\pi r^2 h$, where n is the number density of particles, r the radius of the spheres, and h the vertical thickness of the ring. The mass per unit surface area $\sigma_m = n\rho^4/_3\pi r^3 h$, where ρ is the mass density of a single particle. Clearly we have $r = {}^3/_4\ \sigma_m/\tau\rho$. The estimate of the mass of the rings is $< 3 \times 10^{-6}$ of Saturn's mass (*15*). We assume that most of the mass is in the B ring. This gives $\rho_m < 10^4$ g/cm^2. Taking $\tau > 1.5$ from our results and $\rho \sim 1$, we get $r < 45$ m.

The analysis above applies to ring particles that are all the same size. It seems more likely that a distribution of particle sizes exists. For example, Cuzzi *et al.* (*16*) suggested the distribution $n(r) = n_0 r^{-3}\, dr$ (for $r_1 < r < r_2$). Their model is consistent with results for the breaking up of solids in collisions. The Earth-based optical and radar results indicate that $r_1 \sim 1$ cm (*17*). Putting $r < 45$ m into the model of Cuzzi *et al.* yields $r_2 \lesssim 400$ m. Cuzzi *et al.* showed that the larger particles in the distribution would collapse to form essentially a monolayer, while the smaller particles would be "pumped up" by interactions with the larger ones. The smaller particles thus form a layer many particles thick; the Cuzzi theory then indicates, with our $r < 45$ m, that the ring thickness is < 4 km. Since the main part of the scattering cross section is in the smaller particles, this explains the good agreement of multilayer models with Earth-based data (*14*, *18*).

The ring thickness limit of 4 km is greater, by a factor of ~ 3, than the thickness observed during Earth's ring plane crossing (*18*). We therefore invert the reasoning above and conclude that the typical particle radius $r \lesssim 15$ m and the total ring mass $\lesssim 10^{-6}$ that of Saturn.

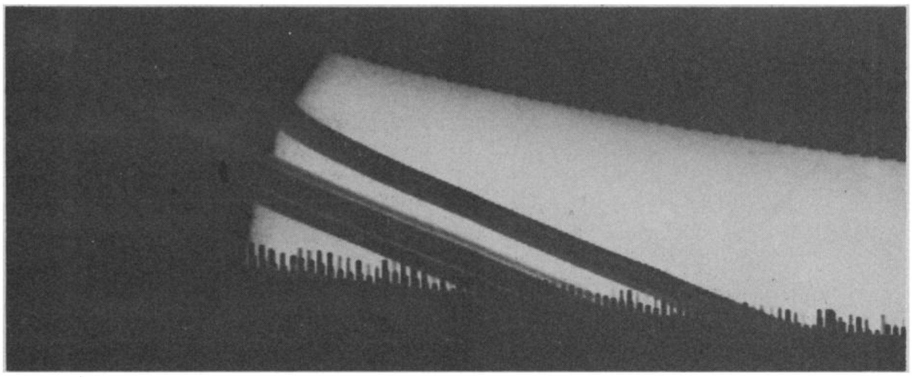

Fig. 4. Image of the rings taken in the red channel on 1 September 1979 at 1132 ERT; range, 395,000 km; latitude, + 3.2°; phase, 13.3°.

From the observations of Fig. 2, not only was the F ring discovered, but a satellite was found that we could not identify with the ephemerides of the numbered satellites (*19*). We therefore assigned it an identification as recommended by the International Astronomical Union (*20*)—namely 1979 S 1, the first Saturn satellite discovered in 1979. The new satellite is also visible in a Pioneer image taken about 10 minutes before Fig. 2. If 1979 S 1 is in the equatorial plane, we find that it is 151,800 ± 600 km = 2.53 ± 0.01 R_S from the center of Saturn in Fig. 2 (see the discussion above of Table 2). The true anomaly, measured in Saturn's equatorial plane from its intersection with Earth's ecliptic, is 66°; this number is rather sensitive to the assumption that the object lies in the equatorial plane.

The satellite, proceeding along its orbit, circled the Saturn system and then nearly collided with the Pioneer spacecraft (*13*). The satellite orbit will be discussed elsewhere (*21*). If we take the radius of the satellite as ~ 100 km from the Chicago and Iowa experiments (*13*), the geometric albedo is 0.18 ± 0.09 in red light. The satellite is too faint to make a reliable determination of its color, but it is seen that the color is not extreme. 1979 S 1 is darker than the other inner satellites (*22*).

Table 2. Listing of objects with their distances from the center of Saturn, in R_S, based on dark-side measurements.

Ring, division, gap, or satellite	R_S
C ring	1.22 to 1.50
French division	1.50 to 1.53
B ring	1.53 to 1.96
Cassini division	1.96 to 2.03
Encke gap	Narrow, 2.21
A ring	2.03 to 2.27
Pioneer division	2.27 to 2.33
F ring	Narrow, 2.33
E ring	Out to 5 or 6
1979 S 1	2.53

Are there any more inner satellites? It is possible that there are, because our coverage at a Channeltron gain as high as that used for Fig. 2 (IPP gain setting 21) is limited.

From preliminary measurements we confirm the equatorial radius of Saturn as 60,000 ± 500 km and derive the ratio of polar to equatorial radii as 0.912 ± 0.006. The IPP determined the orientation of the spacecraft about its spin axis; the usual method, with a special sun sensor on the spacecraft, developed a bias because of the apparent proximity of the sun and Earth at this time, while the star sensor on the spacecraft was out of commission. The photometry and polarimetry were frequently calibrated by observing the star Sirius. The lamp inside the IPP was monitored twice each minute during low-gain polarimetry and a sunlight diffuser mounted in the spacecraft antenna was occasionally observed to detect drifts in the responsivity. Ground-based measurements (*23*) of the brightness of Saturn put the spacecraft data on an absolute photometric scale.

The lack of detail that we see on Saturn, compared to that on Jupiter, is disappointing. We do see some weak evidence for jet stream activity in the Equatorial Zone and also in a high-latitude zone just below the North Polar Region of Saturn. This evidence, which is difficult to reproduce in printed pictures, consists of irregular low-contrast boundaries between the zones and their adjacent belts. The scalloped boundaries appear to be similar to those seen on Jupiter where great differences of jet stream velocities occurred—for instance, between the equatorial region and the North Tropical Zone.

The photometry and polarimetry ob-

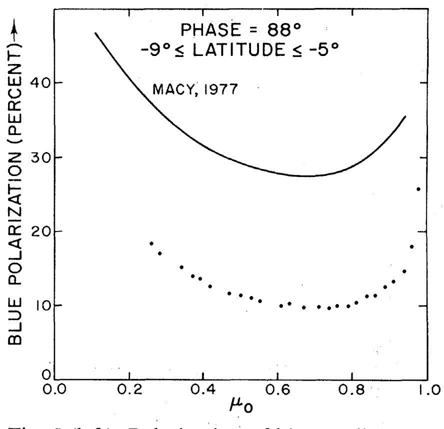

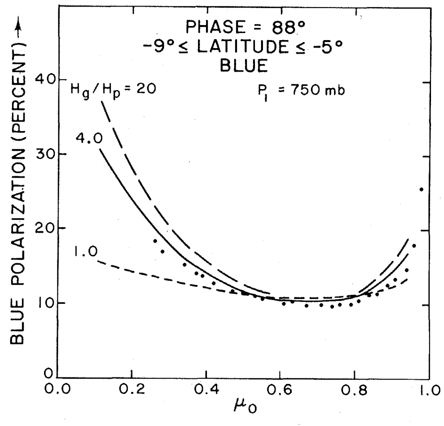

Fig. 5 (left). Polarization of blue sunlight scattered from Saturn's atmosphere as a function of μ_o, the cosine of the solar zenith angle. The points are the observed data; the continuous curve is for the model atmosphere of Macy (*24*). Fig. 6 (right). The data in Fig. 5 compared with models with three different values of H_g/H_p, the ratio of scale heights of gas and particles.

tained for the disk of Saturn will provide useful constraints on the optical properties and vertical distribution of the aerosols in Saturn's atmosphere. These aerosols are expected to be distributed differently on Saturn than on Jupiter. Because the effective temperature of Saturn is some 30 K less than that of Jupiter, the temperature at which the vapor pressure of a possible cloud constituent equals its partial pressure in the atmosphere is reached at significantly greater pressures on Saturn than on Jupiter. Hence NH_3, which can form a cloud near the 600-mbar level on Jupiter, would be expected to have its cloud base on Saturn in the neighborhood of 1 to 3 bars, depending on its mixing ratio. On the other hand, the thermal opacities of both planets are dominated by pressure-induced transitions of H_2, and the tropopause should therefore be reached at similar pressure levels (~ 500 mbar) on both planets. For Jupiter, this means that the NH_3 cloud with its base near ~ 600 mbar may extend to only slightly higher levels, and a relatively thin NH_3 cloud has been included in models of Jupiter constructed by various authors. For Saturn, however, an NH_3 cloud would be expected to have its base at pressures of a few bars, and convection could carry cloud particles to a considerable height above the cloud base—perhaps as high as the 400-mbar level. Indeed, the presence of a deep haze (presumably of NH_3 crystals) has been found to play an important role in explaining the strengths of the visible and near-infrared absorptions of H_2 and CH_4 in models of Saturn's atmosphere (*24*).

To match the variation of the geometric albedo of Saturn with wavelength, Macy (*24*) included a relatively thick layer (τ = 4 at 0.44 μm) of small (radius ≤ 0.1 μm) dark particles between the 200- and 400-mbar pressure levels (just above the top of the NH_3 haze). The size and location of the particles were chosen to minimize the rate of change with wavelength (λ) of the imaginary component of the index of refraction of the particles (which Macy takes as proportional to $\lambda^{-2.5}$) required to give the much lower geometric albedo of Saturn in the blue than in the red. As Macy states, the size and distribution of the absorbing particles that he used are not unique—the particles could be larger or placed deeper if a more rapid variation of imaginary index with wavelength were used. Because the suggested particles are so small and dark and of considerable optical depth, the blue light scattered from the planet near 90° phase angle should be highly polarized perpendicular to the scattering plane, with values of nearly 30 percent at the center of the illuminated portion of the disk. However, Fig. 5 shows the observed polarization of the center of Saturn near 90° phase angle to be little more than one-third of the value in Macy's model; this indicates that the actual particles must be considerably less positively polarizing (hence probably much larger), or the layer very much thinner, than in the model. Indeed, the small polarization (of the order of 2 percent) parallel to the scattering plane that we observe in red light at 88° phase indicates that the optical depth of any positively polarizing aerosols must be negligibly small in the blue also. This suggests that much or most of the polarization seen in blue light could be due to Rayleigh scattering by the gas in the region of the NH_3 haze. From this point of view, the absorbers that make the planet darker in the blue than in the red would be in the region of the NH_3 particles, as they are on Jupiter (*25*), rather than concentrated above it.

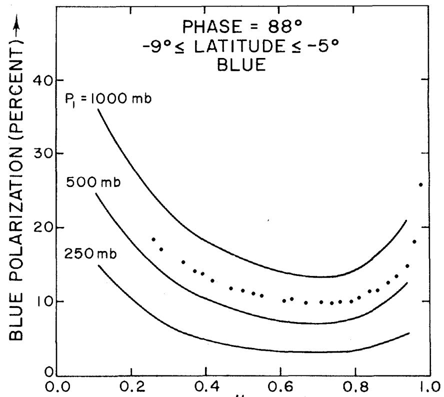

Fig. 7. The data in Fig. 5 compared with three model atmospheres with different values of the pressure, P_1, at which a particle optical depth of unity is reached.

To take a first look at the types of scattering haze models that might fit our polarization data, we used a model with two adjustable parameters. One is the pressure, P_1, at which the optical depth of the aerosols reaches unity. The second is the ratio of the gas scale height to the particle scale height, H_g/H_p. The polarizing properties of the cloud particles are taken to be those we found from our analysis of Jovian clouds (presumably also NH_3 crystals); they have, perhaps coincidentally, about −2 percent polarization for single scattering at 90° phase angle.

Figure 6 shows the variation in computed polarization from the limb nearly to the terminator at 88° phase for a fixed value of P_1 when H_g/H_p is varied from 1 (a homogeneous cloud-gas mixture) to 20 (a sharp cloud top). The amount of polarization near the center of the illuminated portion of the disk is nearly independent of H_g/H_p, but the center-to-limb variation gets rapidly steeper with increasing H_g/H_p. A particle scale height about one-fourth the gas scale height is indicated.

Figure 7 shows the variation of polarization for various values of P_1 with H_g/H_p fixed at 4. The shapes of the curves are relatively insensitive to P_1, but the amount of polarization increases rapidly with increasing P_1. A value of P_1 ~ 750 mbar is indicated.

Actually, the value of P_1 depends somewhat on the single-scattering polarization assumed for the cloud particles; increasing it by 10 percent, at 90° scattering angle, would decrease P_1 by about 100 mbar. After our data at all phase angles in both colors are reduced, we should be able to derive the shape of the single-scattering polarizing properties of the aerosols by requiring a single value of P_1 to give good fits to the data at the center of the disk at all phase angles. If the center-to-limb variation also fits at each phase angle, we can have some confidence in the vertical structure as well. We are obviously still some way from having reduced all our data in both colors and compared it to these types of models; we have approximately 20,000 polarization measurements. Nevertheless, we believe the values derived here for the location of the $\tau = 1$ level of the aerosols and their scale height at equatorial latitudes are reasonably close to the final value we will obtain. The present example demonstrates the usefulness of these data.

T. GEHRELS, L. R. BAKER
E. BESHORE, C. BLENMAN
J. J. BURKE, N. D. CASTILLO
B. DACOSTA, J. DEGEWIJ
L. R. DOOSE, J. W. FOUNTAIN
J. GOTOBED, C. E. KENKNIGHT
R. KINGSTON, G. MCLAUGHLIN
R. MCMILLAN, R. MURPHY
P. H. SMITH, C. P. STOLL
R. N. STRICKLAND, M. G. TOMASKO
M. P. WIJESINGHE
University of Arizona, Tucson 85721
D. L. COFFEEN
Goddard Institute for Space Studies, New York 10025
L. ESPOSITO
Laboratory for Atmosphere and Space Physics, University of Colorado, Boulder 80309

References and Notes

1. T. Gehrels *et al.*, *Science* **183**, 318 (1974).
2. A. L. Baker *et al.*, *ibid.* **188**, 468 (1975).
3. S. F. Pellicori, E. E. Russell, L. A. Watts, *Appl. Opt.* **12**, 1246 (1973). A further discussion of spin-scan imaging is given by E. E. Russell and M. G. Tomasko [in *Chemical Evolution of the Giant Planets*, C. Ponnamperuma, Ed. (Academic Press, New York, 1976)].
4. Review chapters by M. G. Tomasko and T. Gehrels, in *Jupiter*, T. Gehrels, Ed. (Univ. of Arizona Press, Tucson, 1976).
5. P. H. Smith and L. R. Doose, *Sky Telesc.* **58**, 405 (1979).
6. J. J. Burke and R. N. Strickland, in preparation.
7. H. J. Reitsema, *Nature (London)* **272**, 601 (1978).
8. P. Guérin, *Icarus* **19**, 202 (1973).
9. I. R. Ferrín, *ibid.* **22**, 159 (1974).
10. Adjacency effects are due to the lateral diffusion of fresh developer toward a region of higher exposure. The density on the edge of the high-exposure region is therefore increased. The counterflow of developer by-products retards the development in the region next to the high-density edge. See R. S. Barrows and R. W. Wolfe, *Photogr. Sci. Eng.* **15**, 472 (1971).
11. A. F. O'D. Alexander, *The Planet Saturn* (Faber & Faber, London, 1962), p. 178.
12. B. A. Smith *et al.*, *Icarus* **25**, 466 (1975).
13. W. Fillius, W. H. Ip, C. E. McIlwain, *Science* **207**, 425 (1980); J. A. Simpson, T. S. Bastian, D. L. Chenette, G. A. Lentz, R. B. McKibbin, K. R. Pyle, A. J. Tuzzolino, *ibid.*, p. 411; J. A. Van Allen, M. F. Thomsen, B. A. Randall, R. L. Rairden, C. L. Grosskreutz, *ibid.*, p. 415.
14. Y. Kawata and W. M. Irvine, *Icarus* **24**, 472 (1975); L. W. Esposito and K. Lumme, *ibid.* **31**, 157 (1977); ______, W. D. Benton, L. J. Martin, H. M. Ferguson, D. T. Thompson, S. E. Jones, *Astron. J.* **84**, 1468 (1979).
15. J. D. Anderson, G. W. Null, E. D. Biller, S. K. Wong, W. B. Hubbard, J. J. MacFarlane, *Science* **207**, 449 (1980).
16. J. N. Cuzzi, R. H. Durisen, J. A. Burns, P. Hamill, *Icarus* **38**, 54 (1979).
17. J. N. Cuzzi and J. R. Pollack, *ibid.* **33**, 233 (1978).
18. J. W. Fountain and S. M. Larson, *ibid.* **36**, 92 (1978).
19. The position of Janus is unknown for 1979 (that is, the error in orbital phase is > 180°). The satellite discovered by Fountain and Larson (*18*) should be denoted as 1966 S 2, rather than as Saturn 11, as it is sometimes called; its position is also uncertain. The present radius of 2.53 R_S is close to that derived by Fountain and Larson for 1966 S 2.
20. *The International Astronomical Union Circular 3417* of 25 October 1979 has the announcements of 1979 S 1, the F ring, and the Pioneer division.
21. W. H. Blume *et al.*, in preparation. At the Pioneer Project Office, we received considerable help with the problems of the satellite's orbit from J. W. Dyer.
22. D. L. Harris, in *Planets and Satellites*, G. P. Kuiper and B. M. Middlehurst, Eds. (Univ. of Chicago Press, Chicago, 1961), p. 310; D. P. Cruikshank, in *The Saturn System*, D. M. Hunten and D. Morrison, Eds. (Conf. Publ. 2068, National Aeronautics and Space Administration, Washington, D.C., 1977), p. 238.
23. J. Bergstralh and G. Orton, *Bull. Am. Astron. Soc.* **11**, 554 (1979).
24. W. Macy, *Icarus* **32**, 328 (1977).
25. M. G. Tomasko, R. A. West, N. D. Castillo, *ibid.* **33**, 558 (1978).
26. We are indebted for their support to R. P. Hogan and others at the Pioneer Project Office, the Bendix Corporation, and NASA's Deep Space Network, which allowed us to receive the best possible data. We thank Pioneer Project manager C. F. Hall and Pioneer contracting officer J. F. Pogue for supporting the modeling of the Jupiter atmosphere in order to learn for the Saturn encounter. We are also indebted to the Santa Barbara Research Center for the competent design and construction of the instrument, which performed so well over such a long time. Finally, we thank W. B. Hubbard and B. A. Smith for refereeing this report.

3 December 1979

Pioneer Saturn Infrared Radiometer: Preliminary Results

Abstract. *The effective temperature of Saturn, 94.4 + 3 K, implies a total emission greater than two times the absorbed sunlight. The infrared data alone give an atmospheric abundance of H_2 relative to H_2 + He of 0.85 ± 0.15. Comparison of infrared and radio occultation data will give a more precise estimate. Temperature at the 1-bar level is 137 to 140 K, and 2.5 K differences exist between belts and zones up to the 0.06-bar level. Ring temperatures range from 60 to 70 K on the south (illuminated) side and from < 60 to 67 K in the planet's shadow. The average temperature of the north (unilluminated) side is ~ 55 K. Titan's 45-micrometer brightness temperature is 80 ± 10 K.*

Objectives of the infrared radiometer (IRR) experiment are (i) to measure the temperatures and heat balance of Saturn, its rings, and Titan; (ii) to search for horizontal temperature contrast on Saturn; (iii) to infer the atmospheric H_2 to He ratio; and (iv) possibly to infer characteristics of particles in the rings, such as size, thermal inertia, and out-of-plane motion. The instrument, consisting of two broadband channels centered at 20- and 45-μm wavelength, was described in reports following the Jupiter encounters (*1, 2*). The two beams scan at a fixed 75° angle with respect to the forward (that is, away from Earth) spin axis of the spacecraft. A scan consists of 33 observations (words) from a preselected 59° sector of the spacecraft spin cycle. The motion of the spacecraft causes a displacement of scans on the object to be viewed. A simultaneous 20- and 45-μm pair of images were made of Saturn and its rings during the 2.5-hour interval before closest approach (Fig. 1). These ~ 2×10^4 observations (10^4 in each channel), plus about 30 observations during which Titan partly filled the field of view, constitute the IRR data set from the Saturn encounter.

Table 1. Equivalent blackbody temperatures.

Temperature category	Belt (9°S to 12°S)	Zone (0° to 3°S)
T_{20}	91.4 K	89.2 K
T_{45}	99.5 K	97.0 K
$1/2(T_{20} + T_{45})$	95.5 K	93.1 K
T_e (model)	95.6 K	93.2 K
Average T_e	94.4 ± 3 K	

The instrument appears to have functioned correctly during the encounter. The signal when viewing space and the signal when viewing the internal calibration shutter at the known instrument temperature were both normal. The inferred instrument response differed from the laboratory value by less than 3 percent. The noise of a single observation is ± 2 data numbers (DN), equivalent to ± 3.0 K at 20 μm and ± 1.3 K at 45 μm for an object at 100 K, and to ± 3.0 K at 45 μm for an object at 70 K. A brightness temperature of 55 K corresponds to DN(45) = 2.9, which is exceeded 5 percent of the time when viewing space.

The results reported here are preliminary in that we have not computed the instrument pointing from the most recent trajectory analysis, which became available during preparation of this manuscript. For views of the rings at very small instrument elevation angles (for example, near ring plane crossing), and for views of the planet close to the limb, trajectory uncertainties are important.

The data on the Saturn disk were processed by separating them into latitude bins 3° wide, fitting the dependence on emission angle θ to low-order Legendre